RSC Advances

ROYAL SOCIETY OF CHEMISTRY

www.rsc.org/advances

Cobalt(III) Acetylacetonate Initiated RAFT Polymerization of Acrylonitrile and Its Application in Removal of Methyl Orange after Electrospinning

Yuanyuan Xu, Jinming Sun, Hou Chen*, Liangjiu Bai

School of Chemistry and Materials Science, Ludong University, Yantai 264025, China

This study described reversible addition-fragmentation chain-transfer (RAFT) polymerization initiated by cobalt(III) acetylacetonate ($Co(acac)_3$). With $Co(acac)_3$ as the initiator, RAFT polymerization of acrylonitrile (AN) was achieved at 90 ^oC mediated by 2-cyanoprop-2-yl dithionaphthalenoate (CPDN). The polymerization exhibited "living"/controlled characteristics with the molar mass distribution as low as 1.25. The homogeneous polyacrylonitrile nanofibers (PAN-nFs) were produced via electrospinning technique. FTIR, SEM and TGA analysis revealed aminated-PAN-nFs (APAN-nFs) was successfully obtained via ethylenediamine (EDA) grafting onto surface of PAN-nFs. The adsorption interaction between methyl orange (MO) dye and APAN-nFs was discussed in detail. The maximum saturation adsorption capacity was 102 mg/g. The adsorption kinetic followed pseudo-second-order model. Langmuir model was better to interpret the isothermal process for MO of APAN-nFs. The Dubinin-Radushkevich (D-R) isothermal model indicated the adsorption was proceeded chemically. Intraparticle diffusion was not the only rate-limiting step. The thermodynamics properties indicated the adsorption process was exothermic and spontaneous nature. The MO dye adsorbed by APAN-nFs could be reversibly desorbed by the aqueous solution of pH = 1. APAN-nFs could be recycled efficiently.

Introduction

As the development of textile and printing industries, more attention has been payed to the discharge of an enormous amount of anionic dyes into rivers and lakes.[1] It has caused severely bad effect on human beings, aquatic flora and aquatic micro-organisms owning to anionic dyes themselves highly toxic and inhibition the re-oxygenation in water.[2] Consequently, it is extremely urgent to remove or drive down the anionic dyes until their emissions conform to the standard level. Nowadays filtration, reverse osmosis, flocculation, precipitation, evaporation, degradation and adsorption technologies[3-9] have been explored to deal with anionic dyes. Among them, adsorption method, in which fibrous chelating polymers was used as the novel adsorbent, is proved to be reliable and effective technique due to its flexibility, easy operation, low operation cost, and minimum sludge production.[10] Many researchers[11,12] have tried to introduce amino groups into polymers as the anionic dyes can form chelate complexes with these groups. From the point of supramolecular chemistry, anion-chelated complexes are similar but different from host-guest complexes, in which two or more molecules are held together in unique structural relationships by electrostatic forces. Generally, chelate compounds are classified into three categories: corands, cryptands and podands.[13,14] Corands and crytands are dominated by the chelate/macrocyclic effects and the chelate/macrobicyclic effects, respectively, whereas podands are dominated by chelate effect only. Recently, as one typical chelate fiber of the podand type, the polyacrylonitrile (PAN)-based nanofibers (PAN-nFs) is a superior polymer for

introducing amino groups. The modified PAN-based nanofibers (PAN-nFs) have attracted more attention for high porosity, high gas permeability, and most importantly large surface area per unit mass.[15,16]

Generally, the nFs can be easily produced by electrospinning technique since electrical forces were first applied to polymeric filaments by Anton Formalas.[17] Compared with conventional physical-chemical methods (molecule self-assemblies, physical vapor deposition, etc.), electrospinning technique distinguishes itself due to its simple devices, and manufacture one-dimensional (1D) nanomaterials with high slenderness ratio.[18-21] To the best knowledge of us, the commercial available PAN-nFs are prone to lousiness, tangle and fracture which are prepared by traditional radical polymerization (RP) methods with relatively lower molecular weights (MW) and poorly controlled over molecular weight distributions (MWDs).[22] Theoretically, PAN with relatively broader MWDs usually has a wide distribution of the hydrodynamic radii and relaxation times of the chains in solution. During the process of PAN stretching, the presence of the relatively small PAN chains that have a smaller hydrodynamic volume and consequently a lower local chain entanglement density, acts as a weak link that causes a premature break-up of local 'chain-chain coupling' within the jet resulting in the formation of PAN droplets.[23] Compared with those synthesized by RP techniques, electrospinning of polymers based upon reversible-deactivation radical polymerization (RDRP) techniques can produce continuous nFs that are exceptionally long in length and uniform in diameter with inherent excellent control over MW and MWDs. Providing that PAN was

monodisperse, all the PAN chains in solution have nearly the same hydrodynamic volume that results in a very sharp spectrum of the relaxation times. It is a key element for PAN stretching process induced by the electrically driven bending instabilities during electrospun fiber formation process.[24]

Among RDRP systems, transition metal salts, especially cobalt compounds,[25-29] have exerted "living"/controlled roles in polymerizing reactive vinyl monomers. Greatly different from cobalt(II) acetylacetonate ($Co(acac)_2$)-capped chains by C-Co σ bond, cobalt(III) acetylacetonate ($Co(acac)_3$) can act as initiator due to generation of acetyl acetone group (acac).[30] Actually, transition metal acetylacetonate ($Mt(acac)_x$) has successfully initiated the polymerization of styrene (St) in combination with organic halide (R-X).[31] Of particular note is that the MWD of PS mediated by $Co(acac)_3$/benzyl bromide (BzBr) was as high as 1.63 due to occurrence of chain transfer reaction and bi-radical termination.[30] However, unlike the reactive monomers (MMA, St, etc.), acrylonitrile (AN) is special for its strong polarity of cyano, causing negative effect on the conjugated structure. As a result, it is a more challenging project for polymerizing well-defined polyacrylonitrile (PAN) mediated by $Mt(acac)_x$. On the other hand, addition of chain transfer agents (CTAs) into RP method can obtain well-defined polymers, namely reversible addition-fragmentation chain-transfer (RAFT) polymerization technique.[32-35] Several kinds of RAFT agents have been appropriately applied to synthesis of PAN and its copolymers in the presence of azo-initiators.[36-38] Whereas, only manganese acetylacetonate ($Mn(acac)_3$) has been reported as the initiator in polymerization of AN with RAFT agent in our

research group until now.[39] In this work, we first synthesized PAN with $Co(acac)_3$ as the initiator instead of azo compounds and CPDN as the RAFT agent. PAN-nFs were produced using electrospinning technique. The adsorbent APAN-nFs was obtained after amination upon PAN-nFs. The material possessed well chelating ability with dyes and MO adsorption and desorption were discussed in detail.

.

Results and discussion

Preparation of the adsorbent APAN-nFs

The polymerization of AN was discussed in detail, which can be taken from Tables TS1-TS2, Fig. S1-S4, ESI†. The homogeneous PAN-nFs, the PAN polymer with the narrowest molecular weight distribution (M_w/M_n = 1.25) was selected to be the electrospinning precursor. The concentration of PAN in DMF was set to be 10%. The homogeneous solution was spun on an electrospinning apparatus. The ideal synthetic route of the adsorbent APAN-nFs that was aminated by EDA onto the surface of PAN-nFs was illustrated in Scheme 1. The nitrogen content was observed as 28%, 42%, 56% at 5 h when the temperature was 90 ^oC, 100 ^oC, and 110 ^oC, respectively. The conversion of nitrile group in PAN-nFs increased with increasing temperature, which was attributed to the endothermic nature of the reaction. The result was the same as that in Mehdi Rafizadeh's research group.[40] The presence of functional groups was confirmed by FTIR, as illustrated in Fig. 1. The intensity of distinctive stretching vibration of **C≡N** at 2241 cm^{-1} became weaker in APAN-nFs (Fig. 1 (b)

and (c)) than that of PAN-nFs (Fig. 1 (a)). Furthermore, the stretching vibration of **C≡N** became much weaker (Fig. 1 (b) vs. (c)) when the modification was proceeded at the relatively higher temperature, indicating that the reaction was quantitative at 110 ^{o}C. The peak at 3550 cm^{-1}, which was attributed to N-H stretching vibration, increased in intensity of APAN-nFs (Fig. 1 (b) and (c)) compared with that in PAN-nFs (Fig. 1 (a)). Besides, the intense of absorption band at 1650 cm^{-1} increased, compared with Fig. 1 (b), (c) and (a), attributing to the formation of amidine group N-C=N. As a result, it suggests that the nitrile group of PAN-nFs was modified successfully and the relatively higher temperature was more feasible in terms of modification. At first, PAN-nFs appeared to be flexible and white in color. Whereas, their appearance changed with the increasing modified temperatures. The color of fibers was observed to change from white to light yellow to pale orange when the grafting process was conducted at 90 ^{o}C, 100 ^{o}C, and 110 ^{o}C, respectively. Furthermore, APAN-nFs became fragile with relative higher temperature. It laid solid foundation for adsorption of MO that large amounts of chelating sites were presented by APAN-nFs. SEM exhibits the appearance of PAN-nFs and APAN-nFs obtained at high and low magnification, as shown in Fig. 2. Though the micrograph and diameter distributions of APAN-nFs modified at 110 ^{o}C (Fig. 2 (C) and (D)) were similar to those of PAN-nFs (Fig. 2 (A) and (B)), the nanofiber mats were observed to slightly contract in size. This effect was based on the physical nature of the thread and fibers which make up the thread. In order to manufacture an elongated form, the fibers were produced by a hot extrusion process via electrospinning technique. PAN-nFs were

known to be in a high energy metastable state. While subjected to a wet heating process, PAN-nFs relaxed to a lower energy state. Consequently, the fibers would contract.[40] On the other hand, APAN-nFs were insoluble in DMF even after 15 days while the comparable amount of PAN-nFs possessed excellent solubility after 0.5 h under the same conditions. It indicates that the interior of APAN-nFs was cross-linked to some extent. As was reported,[41] PAN-nFs segments in low-order area started relaxation at 90 ^{o}C, rendering solution into amorphous region. Hence increasing contact between EDA and PAN-nFs. When the temperature reached 105 ^{o}C or even higher, sequence chain segment in amorphous region began to move and PAN-nFs exhibited obvious swelling property. EDA could easily pass into PAN-nFs interior, resulting in formation of crosslinking structure. It was consistent with the results reported in Abdouss' research group and patent invented by Borrell's research group.[42-44] Thermal stabilities of PAN-nFs and its aminated derivative APAN-nFs at different temperatures were conducted under nitrogen atmosphere at a heating rate of 10 K/min (Fig. 3). PAN-nFs showed multistage thermogravimetric profiles as shown in Fig. 3 (a). The first weight loss was slight due to the production of ammonia gas and hydrogen cyanide during the cyclization process within 150 ^{o}C. While the second was serious due to amounts of hydrogen and methane volatilization in the course of cyclic structures decomposition from 280 ^{o}C to 500 ^{o}C. Compared with Fig. 3 (a), though the peaks weakened, there were still two weight loss peaks in Fig. 3 (b) owning to the incomplete modification at 90 ^{o}C. When the modification proceeded under 110 ^{o}C, as shown in Fig. 3 (c), only one weightless peak was presented between

270 ^{o}C and 500 ^{o}C. It may be caused by damage of nitrile groups after amination, rendering failure of cyclization.

Adsorption capacity

Investigation of the adsorption interaction under various pH solution

Firstly, adsorption experiments of the selected three dyes, i.e. MO, MB and FSS, were conducted with the same concentration of 4×10^{-4} mmol.mL^{-1} at 20 ^{o}C in the aqueous solution, respectively. As exhibited in Fig. 4, APAN-nFs showed the maximum adsorption capacity towards MO in contrast with MB and FSS. The minimum adsorption capacity of FSS attributed to itself as one cationic dye. As a result, MO was the optimal candidate in the following experiments.

Fig. 5 shows the adsorption kinetics of MO onto APAN-nFs in different pH solutions at 20 ^{o}C. As can be seen from Fig. 5 that the adsorption capacity was the lowest when it was in 1 mol.L^{-1} HCl solution. The loading ability reached the optimal level when the experiments were proceeded in 1 mol.L^{-1} NaOH solution and NaCl solution, respectively. The adsorption capacity was moderate in aqueous solution. As was reported[1,14,45] that electrostatic force, hydrogen bond (HB) and hydrophobic force were the predominant interactions during the adsorption process. The suppression of electrostatic attraction and enhancement of hydrophobic attraction will occur when the ionic strength increases. Whereas, the ionic strength slightly affects the HB. When the experiment was conducted in 1 mol.L^{-1} HCl solution, most of the functional groups such as -NH- were protonated and presented in the positively charged form

and MO existed as quinone form, generating that the electrostatic repulsion (ER) far exceeded the electrostatic attraction (EA). Furthermore, acidifying APAN-nFs reduced the number of active binding sites. Hence obtaining minimum adsorption capacity for MO onto APAN-nFs at low pH. Therefore, the adsorption of MO in acidic solution was unfavorable. The HA increased with the enhancement of ionic strength in a relatively higher pH solution. The presence of HB, as another important element, increased the adsorption capacity in NaCl solution as well. As a result, the enhancement of hydrophobic attraction (HA), weakening of ER and existence of HB boosted the loading ability of MO onto APAN-nFs. Therefore, the probable interaction between adsorbate MO and adsorbent APAN-nFs was proposed, as illustrated in Scheme 2.

Adsorption kinetics

Adsorption kinetics is one of the important parameters for the adsorbents practical application due to its evaluation of the uptake rate and contact time for dyes. Fig. 6 shows the results of different concentrations of MO (4×10^{-4} mmol.mL^{-1}, 8×10^{-4} mmol.mL^{-1}, and 16×10^{-4} mmol.mL^{-1}) adsorption onto the APAN-nFs as a function of time under 20 ^{o}C. The changes in contact time exhibited approximately the same effect on various concentrations of MO. The amount of MO onto the APAN-nFs increased rapidly at the first 12 h and then levelled off. As a result of the adequately available active adsorption sites for the high specific surface area, the adsorption rates were rapid initially upon different concentrations of MO. Thereafter it continued at a

much slower rate and finally reached equilibrium due to saturation of APAN-nFs surface sites. Thus the kinetics adsorption provided a powerful basis to define the optimum contact time.

The adsorption mechanism of APAN-nFs upon MO was evaluated by utilizing commonly used kinetics models, i.e. the pseudo-first-order model and pseudo-second-order model. The equations were expressed as follows:[46,47]

$$\log\frac{q_e - q_t}{q_e} = -k_1 t \quad (3)$$

$$\frac{t}{q_t} = \frac{1}{k_2 q_e^2} + \frac{t}{q_e} \quad (4)$$

Wherein, q_e (mmol.g^{-1}) and q_t (mmol.g^{-1}) represent the amounts of MO adsorbed on the APAN-nFs at the equilibrium and any time t, respectively. k_1 (min^{-1}) and k_2 (g (mmol.min)$^{-1}$) are the rate constants of pseudo-first-order and pseudo-second-order, respectively.

Compared with Fig. 7 (a) and (b), the linear graphs indicate that the kinetics data fitted better to pseudo-second-order model. The result was further confirmed by the proof that (Table 1) correlation coefficients in pseudo-second-order model ($R^2 > 0.99$) were much closer to 1.0 than those in pseudo-first-order model. These results suggest that the adsorption of MO onto the surface of APAN-nFs followed pseudo-second-order kinetic model.

Adsorption isotherms

Adsorption isotherms is one important parameter for interpretation of the interactive behavior between adsorbate and adsorbent. It is critical in optimizing the application

of an adsorbent as well. Fig. 8 presents adsorption amounts of MO onto APAN-nFs after the equilibrium time as a function of equilibrium concentrations under different temperatures. Adsorption showed rapid increase initially, as the concentration of MO increased, the adsorption capacity levelled off. The initial increase was related to the large number of chelating amine sites that were presented on APAN-nFs, as well as the high specific surface area of the nFs. The adsorption equilibrium can be constructed as a relation of the adsorbate concentration on the surface of APAN-nFs and in the solution at the given temperature. As can be seen from Fig. 8 that the adsorption capacity for MO of APAN-nFs was lowered as the temperature increased. This indicates that the adsorption process was exothermic. Furthermore, the loading capacity of APAN-nFs for MO increased with the increasing initial MO concentrations as a result of greater driving force by a higher concentration gradient pressure.

In order to further interpret the adsorption mechanism and assess the adsorption characteristics, the isotherms data were analyzed by Langmuir and Freundlich models. The equations were listed as follows:[48,49]

$$\frac{C_e}{q_e} = \frac{C_e}{q} + \frac{1}{qK_L} \quad (5)$$

$$\ln q_e = \ln K_F + \frac{\ln C_e}{n} \quad (6)$$

Where q_e (mmol.g^{-1}) and C_e (mmol.mL^{-1}) stand for adsorption capacity and concentration of dyes in a state of equilibrium, respectively. q (mmol.g^{-1}) is maximum adsorption amount, K_L (mL.mmol^{-1}), an empirical constant which is related to the binding energy. n ((mL.mmol^{-1})^n), the Freundlich constant which is corresponding to

adsorption intensity, K_F (mmol.g^{-1}), the combination ability of chemical bond between adsorbent and dyes.

As shown in Fig. 9 (a) and (b), Langmuir model was better to describe the adsorption isotherm results for MO of APAN-nFs than Freundlich model. The important parameters were calculated as listed in Table 2. Among them, the correlation coefficients of Langmuir model ($R^2 > 0.99$) were closer to 1.0 than those of Freundlich model. According to Langmuir model theory, adsorption occurs at specific homogeneous sites. In other words, no further adsorption can occur at this site once a sorbate occupies a chelate site. Therefore, the adsorption of MO took place via the formation of a monolayer.

Moreover, the favorability of adsorption for MO in case of Langmuir model is determined by the dimensionless separation factor R_L. It was calculated based on the equation as follows:[15]

$$\mathbf{R_L = \frac{1}{1+K_L C_0}} \quad (7)$$

Where K_L (mL.mmol^{-1}) is an empirical constant of Langmuir model. C_0 (mmol.mL^{-1}) represents the initial concentration of dyes.

The values of R_L can be classified into three categories: I $R_L > 1$, II $0 < R_L < 1$, III $R_L = 0$, suggesting that adsorption is unfavorable, favorable, and irreversible, respectively. The R_L values approximately decreased from 0.70 to 0.10 with the increasing initial concentration of MO at various temperatures, as presented in Fig. 10. This indicates that MO adsorption was more favorable at higher initial concentration of MO.

The equilibrium data were also fitted by D-R isothermal model to determine the nature of adsorption process as physical or chemical. The linear from of D-R isotherm equation is listed as follows.[50,51]

$$\ln q_e = \ln q_m - \beta\varepsilon^2 \quad (8)$$

where β ($mol^2.J^{-2}$) is the activity coefficient corresponding to adsorption mean free energy. ε is Polanyi potential which can be listed as equation (9):

$$\varepsilon = RT \ln\left(1 + \frac{1}{Ce}\right) \quad (9)$$

The mean free energy E ($kJ.mol^{-1}$) is calculated by using the value of β according to the following equation.

$$E = \frac{1}{\sqrt{2\beta}} \quad (10)$$

The value of E as the judgment standard to access the adsorption mechanism as physical or chemical. If the E value is below 8 $kJ.mol^{-1}$, the adsorption proceeds physically. If it lies between 8 and 16 $kJ.mol^{-1}$, the adsorption takes place chemically. The fitting parameters of D-R model and the calculated E values are listed in Table 5. As is shown in Table 3, all the E values were about 10.00 $kJ.mol^{-1}$, suggesting the adsorption of MO was carried out by chemical mechanism.

A typical liquid/solid adsorption generally involves film diffusion, intraparticle diffusion and mass action. As for physical adsorption, mass action is a very swift process. As demonstrated above, the adsorption mainly proceeded with chemical mechanism. Consequently, mass action could be neglected and the adsorption diffusion models in this study are mainly based on film diffusion and/or intraparticle diffusion. The diffusion mechanism is studied by the intraparticle diffusion model, as

shown in equation (11).[52]

$$q_t = K_d t^{1/2} \quad (11)$$

where K_d is the diffusion coefficient value.

This model assumes that the plots of q_t versus $t^{1/2}$ should yield a straight line through the origin provided that the intraparticle diffusion is the only rate-controlling step. Fig. 11 shows non-linear plots of q_t versus $t^{1/2}$ for MO, indicating that intraparticle transport is not the only diffusion mechanism. The plot of the whole range is divided into three distinct parts. The first sharp region shows adsorption, however, in the second region besides adsorption, diffusion occurred attributing to layers between fibers. The third part exhibited equilibrium phase because of the rate decrease of saturation intraparticle diffusion.

In order to evaluate the thermodynamic feasibility and spontaneous nature for the MO adsorption onto APAN-nFs, the thermodynamic parameters for the adsorption process such as Gibbs free energy changes ($\triangle G$), enthalpy change ($\triangle H$) and entropy change ($\triangle S$) were calculated according to the equations as follows.[53,54]

$$\log K_c = \frac{\triangle S}{2.303R} - \frac{\triangle H}{2.303RT} \quad (12)$$

$$\triangle G = \triangle H - T\triangle S \quad (13)$$

Wherein, K_c represents the distribution coefficient which is calculated as the ratio of MO equilibrium concentration in the adsorbents and aqueous phases. T (K) is the absolute temperature and R (8.314 $J.mol^{-1}.K^{-1}$) is the gas constant. $\triangle H$ and $\triangle S$ can be obtained via the slope and intercept of the linear plot of $\log K_c$ versus 1/T. Fig. 12 exhibits the linear relationship between $\log K_c$ and 1/T and the calculated

thermodynamic parameters are listed in Table 4. The negative value of $\triangle H$ demonstrates that the adsorption process was exothermic, implied that increasing temperatures may inhibit the adsorption of MO onto APAN-nFs. The phenomenon was consistent with that in the adsorption isotherms. The positive value of $\triangle S$ reveals that randomness was increased at the solid-solution interface during the adsorption of MO process. The negative values of $\triangle G$ implied that the adsorption process was spontaneous at different temperatures. The values of $\triangle G$ decreased with the increasing temperature, indicating that the adsorption process was more feasible at the relatively lower temperature. In conclusion, the thermodynamic implies the adsorption process of MO onto APAN was spontaneous and can be promoted by decreasing the temperature.

Dye desorption and reuse of the fibers

From the discussion above, it is known that electrostatic force, HB and hydrophobic force were the main interactions of MO adsorption by APAN-nFs. The numbers of positive and negative charges of APAN-nFs can be controlled through contacting with different pH solution. It is rational that the adsorbed MO can be released simply through contacting with different pH solution. When the adsorption process was proceeded at strong acid conditions, acidifying APAN-nFs presented in the positively charged form and MO existed as quinone form, enhancing ER between MO and APAN-nFs. Therefore, the desorption and adsorption experiments for MO were mainly performed at relatively lower pH and higher pH solution. Fig. 13 shows

that the dyes adsorption performances of APAN-nFs exhibited a certain degree of loss after the first time reuse, and then it levelled off. A conclusion can be drawn that the adsorbent APAN-nFs possessed reusability.

Experimental section

Materials

Acrylonitrile (AN, > 98.5%, Tianjin Fuchen Chemical Reagent Co., Tianjin, China) was purified via atmospheric distillation prior to being conserved at 5 ^{o}C. Cobalt(III) acetylacetonate ($Co(acac)_3$, > 98.0%, Aladdin) was used without further purification. 2-Cyanoprop-2-yl dithionaphthalenoate (CPDN) was synthesized according to the literature reported elsewhere.[55] *N,N*-dimethylformaide (DMF, > 99.5%, Tianjin Bodi Chemical Reagents Co., Tianjin, China) was dealt with molecular sieves to eliminate water. Methyl orange (MO, A.R. grade, Tianjin Damao Chemical Reagent Co., Tianjin, China), ethylenediamine (EDA, A.R. grade, Tianjin Fuyu Fine Chemical Co., Tianjin, China), ethanol (A.R. grade, Laiyang Economic and Technological Development Fine Chemical Co., Yantai, China), methanol (A.R. grade, Tianjin Damao Chemical Reagent Co., Tianjin, China), and lithium bromide (LiBr, > 98.0%, Tianjin Guangfu Fine Chemical Insititute, Tianjin, China) were used as received.

Apparatus and instrumentation

The number-average molecular weights (M_n) and molecular weight distributions (M_w/M_n) of obtained polymers were determined by Waters 1515 gel permeation chromatograph

(GPC) assembled with a refractive-index detector (Waters 2414) using HR column (7.8 × 300 mm). DMF with 0.1 M LiBr was used as the eluent at a flow rate of 1.0 mL/min and 35 ^{o}C. The concentration of MO was measured by UV-vis spectra analyses, assembled with a Shimadzu UV 2550 spectrophotometer over the wave number range of 350-550 cm^{-1}, according to Lambert-Beer law. The PAN-nFs were obtained by the electrospinning apparatus (Beijing Fuyouma Science and Technology Ltd., Beijing, China), mainly composed by a 10 mL glass syringe, needle tips with different sizes, a high voltage power supply, and a stainless steel drum as the collector. The thermostabilities of the PAN-nFs and APAN-nFs were measured based on thermogravimetric analysis (TGA, Netzsch TG 209, Germany). The chemical or physical interactions were analyzed by infrared spectra Perkin-Elmer Spectrum 2000 FTIR (MAGAN550, Nicolet, America) using the KBr pellet technique. The surface morphologies of samples were characterized by high and low vacuum scanning electron microscopy (SEM, JSM-5610LV, Tokyo, Japan), operating at 20 kV.

Preparation of the adsorptive membrane

PAN polymer with the narrowest M_w/M_n was the optimal candidate for electrospinning. PAN/DMF solution, with concentration (wt%) of 10%, was put into vacuum drying oven until the homogeneous solution was obtained at room temperature. To produce a web, a voltage of 18 kV was applied to the tip of needle and collector, and the distance between them was 15 cm. The feeding rate of the PAN solution was 190 uL/h. The electrospinning procedures were conducted under the

ambient temperature. The PAN-nFs were collected on a stainless steel drum in the form of non-woven mat. Afterwards, 2 g of PAN was immersed in the mixture of 100 mL EDA at 90 ~ 110 ^{o}C for 5 h. The resulting material (APAN-nFs) was extracted by ethanol for 12 h until the pH reached 7. It was dried at 60 ^{o}C under vacuum for 24h until the constant weight was recorded at room temperature.

The degree of -CN group conversion to an amine group was calculated by gravimetry. The conversion percent was calculated as follows:

$$\text{Graft yield}(\%) = \frac{m_1 - m_0}{m_0} \times \frac{M_0}{M_1} \times 100 \quad (1)$$

Wherein, m_0 (g) and m_1 (g) represent the weight of PAN-nFs and APAN-nFs, respectively. M_1 and M_0 are the molar mass of EDA (60.10 g.mol^{-1}) and AN monomer (53.06 g.mol^{-1}), respectively.

Adsorption dynamic experiments

The adsorption kinetics was proceeded using batch method. The equivalent amount of APAN-nFs and MO, methylene blue (MB), fluorescein sodium (FSS) were mixed, respectively, with the same concentration of 4×10^{-4} mmol.mL^{-1} at aqueous solution under 20 ^{o}C. Subsequently, to investigate the adsorption mechanism, the adsorption kinetics of MO were conducted under 1 mol.L^{-1} hydrochlric (HCl) solution, 1 mol.L^{-1} sodium hydroxide (NaOH) solution, 1 mol.L^{-1} sodium chloride (NaCl) solution, respectively. Furthermore, appropriate amount of APAN-nFs and different concentrations of MO solution (4×10^{-4} mmol.mL^{-1}, 8×10^{-4} mmol.mL^{-1}, and 16×10^{-4} mmol.mL^{-1}) were mixed together to perform the kinetics experiments under 20

^{o}C. After certain time intervals, some solution was withdrawn and the concentrations of MO in solution were determined with UV spectrum. The adsorption capacity of APAN-nFs for MO was calculated based on the equation as follows:

$$q = \frac{(C_0 - C_e)VM}{m} \quad (2)$$

Wherein, q (mg.g^{-1}) is the amount of MO adsorbed per unite mass of APAN-nFs. C_0 (mmol.mL^{-1}) and C_e (mmol.mL^{-1}) are the initial and equilibrium concentration of MO, respectively. *M* (327.33 g.mol^{-1}) is the relative molecular mass of MO. V (mL) is the solution volume. m (g) stands for the weight of APAN-nFs.

Adsorption thermodynamics experiments

In order to investigate the thermodynamics experiments, appropriate amount of APAN-nFs and various concentrations of MO solution from 1 × 10^{-4} mmol.mL^{-1} to 16 × 10^{-4} mmol.mL^{-1} were mixed, respectively. A certain volume of supernatant under different temperatures was collected to evaluate concentrations of MO by UV spectrum. The calculation of adsorption capacity was based on equation (2).

Desorption and reuse of the APAN-nFs

Into 100 mL of MO solution (pH = 7) certain amount of fibers were added. When the adsorption equilibrium was reached, the adsorpbent APAN-nFs was taken out and put into 10 mL of deionized water with pH 1. The mixture was stirred gently. After certain time for MO desorption, APAN-nFs was taken out and washed several times by water until pH = 7. Then APAN-nFs was immersed into the MO solution again for

the re-adsorption.

Conclusions

In this work, PAN was first successfully synthesized utilizing $Co(acac)_3$ in combination with CPDN. The polymerization proceeded in a well "living"/controlled manner. $Co(acac)_3$ and CPDN were proved to be the highly efficient initiator and CTA, respectively. The MWD of the obtained PAN was as low as 1.25. The diameter of PAN-nFs was evenly distributed at 300 nm. EAD was successfully grafted onto the surface of PAN-nFs without reduction in sample (APAN-nFs) flexibility. The maximum adsorption capacity for MO of APAN-nFs was 102 mg/g. As for the adsorption interaction between MO and APAN-nFs, EA and ER played dominant roles at relatively lower pH. HA and HB were the key elements that affected the adsorption capacity of MO with addition of NaCl or NaOH. The adsorption kinetic followed pseudo-second-order model. Langmuir model was better to interpret the isothermal process for MO of APAN-nFs. The E values calculated from D-R model implied the adsorption took place by chemical mechanism. Negative $\triangle G$ and $\triangle H$ suggested the spontaneous and exothermic nature of the adsorption process. MO adsorbed by APAN-nFs could be reversibly desorbed at pH = 1 solution. The adsorbent showed reused ability as well. The results showed that APAN-nFs, with PAN synthesized via RAFT technique as the precursor, was the promising candidate materials for the removal of MO dyes.

Acknowledgments

The authors are grateful for the financial support by the Program for New Century Excellent Talents in University (No. NCET-11-1028), the Natural Science Foundation for Distinguished Young Scholars of Shandong province (No. JQ201203), and the Program for Scientific Research Innovation Team in Universities of Shandong Province.

References

1. Y. Hu, T. Guo, X. Ye, Q. Li, M. Guo, H. Liu and Z. Wu, *Chem. Eng. J.*, 2013, **228**, 392.
2. Y. Zhang, R. Qu, C. Sun, C. Ji, H. Chen and P. Yin, *Chem. Eng. J.*, 2015, **270**, 110.
3. N. Saffaj, H. Loukili, S. A. Younssi, A. Albizane, M. Bouhria, M. Persin and A. Larbot, *Desalination*, 2014, **168**, 301.
4. S. K. Nataraj, K. M. Hosamani and T. M. Aminabhavi, *Desalination*, 2009, **249**, 12.
5. E. Guibal and J. Roussy, *React. Funct. Polym.*, 2007, **67**, 33.
6. A. Martinez-de La Cruz and S. O. Alfaro, *J. Mol. Catal. A: Chem.*, 2010, **320**, 85.
7. S. Yang, L. Zhang, Q. Yang, Z. Zhang, B. Chen, P. Lv, W. Zhu and G. Wang, *J. Mater. Chem. A*, 2015, **3**, 7950.
8. J. Zhang, Z. Xiong and X. S. Zhao, *J. Mater. Chem.*, 2011, **21**, 3634.
9. W. W. Ngah, L. C. Teong and M. A. Hanafiah, *Carbohyd. Polym.*, 2011, **83**, 1446.
10. G. Crini and P. M. Badot, *Prog. Polym. Sci.*, 2008, **33**, 399.
11. N. Sakkayawong, P. Thiravetyan and W. Nakbanpote, *J.Colloid Interf. Sci.*, 2005, **286**, 36-42.
12. M. S. Chiou and H. Y. Li, *Chemosphere*, 2003, **50**, 1095.

13. J. W. Steed, J. L. Atwood, 1st ed., John Wiley & Sons, Chichester 2000.

14. Y. G. Ko, U. S. Choi, T. Y. Kim, D. J. Ahn and Y. J. Chun, *Macromol. Rapid Comm.*, 2002, **23**, 535.

15. P. K. Neghlani, M. Rafizadeh and F. A. Taromi, *J. Hazard. Mater.*, 2011, **186**, 182.

16. K. Saeed, S. Haider, T. J. Oh and S. Y. Park, *J. Membr. Sci.*, 2008, **322**, 400.

17. A. Formhals, Process and apparatus for preparing artificial threads. USA patent No, 1,975,504, 1934.

18. D. H. Reneker and I. Chun, *Nanotechnology*, 1996, **7**, 216.

19. B. Ortaç, F. Kayaci, H. A. Vural, A. E. Deniz and T. Uyar, *React. Funct. Polym.*, 2013, **73**, 1262.

20. J. A. Matthews, G. E. Wnek, D. G. Simpson and G. L. Bowlin, *Biomacromolecules*, 2002, **3**, 232.

21. S. Niu, L. Zhang, N. Wang, J. Zhu, W. Zhang, Z. Cheng and X. Zhu, *React. Funct. Polym.*, 2013, **73**, 1447.

22. S. Niu, L. Zhang, J. Zhu, W. Zhang, Z. Cheng and X. Zhu, *J. Polym. Sci., Part A: Polym. Chem.*, 2013, **51**, 1197.

23. L. Tan, J. Pan and A. Wan, *Colloid Polym. Sci.*, 2012, **290**, 289.

24. P. Gupta, C. Elkins, T. E. Long and G. L. Wilkes, *Polymer*, 2005, **46**, 4799.

25. Y. Piette, A. Debuigne, C. Jérôme, V. Bodart, R. Poli and C. Detrembleur, *Polym. Chem.*, 2012, **3**, 2880.

26. C. M. Liao, C. C. Hsu, F. S. Wang, B. B. Wayland and C. H. Peng, *Polym. Chem.*, 2013, **4**, 3098.

27. I. Allaoua, B. E. Goi, M. M. Obadia, A. Debuigne, C. Detrembleur and E. Drockenmuller, *Polym. Chem.*, 2014, **5**, 2973.

28. A. Debuigne, C. Michaux, C. Jérôme, R. Jérôme, R. Poli and C. Detrembleur, *Chem. Eur. J.*, 2008, **14**, 7623.

29. A. Debuigne, R. Poli, C. Jérôme, R. Jérôme and C. Detrembleur, *Prog. Polym. Sci.*, 2009, **34**, 211.

30. K. Endo and A. Yachi, *Polym. Bull.*, 2001, **46**, 363.

31. M. A. Tasdelen, Y. Yagci, A. L. Demirel, T. Biedron and P. Kubisa, *Polym. Bull.*, 2007, **58**, 653.

32. J. Chiefari, Y. K. Chong, F. Ercole, J. Krstina, J. Jeffery, T. P. Le, R. Mayadunne, G. F. Meijs, C. Moad, G. Moad, E. Rizzardo and S. H. Thang, *Macromolecules*, 1988, **31**, 5559.

33. S. T. Hemp, A. E. Smith, W. C. Bunyard, M. H. Rubinstein and T. E. Long, *Polymer*, 2014, **55**, 2325.

34. S. Chen and W. H. Binder, *Polym. Chem.*, 2015, **6**, 448.

35. D. J. Keddie, *Chem. Soc. Rev.*, 2014, **43**, 496.

36. Q. An, J. Qian, L. Yu, Y. Luo and X. Liu, *J. Polym. Sci., Part A: Polym. Chem.*, 2005, **43**, 1973.

37. X. H. Liu, G. B. Zhang, B. X. Li, Y. G. Bai, D. Pan and Y. S. Li, *Eur. Polym. J.*, 2008, **44**, 1200.

38. Z. Yue, D. X. Wang, J. Q. Liu, J. Zhang, S. Y. Feng, *Chinese Chem. Lett.*, 2012, **23**, 989.

39. Y. Xu, J. Sun, H. Chen, L. Bai, Q. Tao, L. Yu and Y. Wang, *J. Polym. Sci. Part A: Polym. Chem.*, 2015, **53**, 1305.

40. P. K. Neghlani, M. Rafizadeh and F. A. Taromi, *J. Hazard. Mater.*, 2011, **186**, 182.

41. Y. Fan, H. J. Liu, Y. Zhang and Y. Chen, *J. Hazard. Mater.*, 2015, **283**, 321.

42. P. Tahaei, M. Abdouss, M. Edrissi, A. M. Shoushtari and M. Zargaran, *Materialwiss. Werkst.*, 2008, **39**, 839.

43. A. M. Shoushtari, M. Zargaran and M. Abdouss, *J. Appl. Polym. Sci.*, 2006, **101**, 2202.

44. P. Borrell, P. D. Harrison, and J. C. Marriott, Cationic Fibers Suitable for Ion-exchange Materials and their Production. Eur. Pat., 0,194,766, A1.

45. M. Meot-Ner, *Chem, Rev.*, 2005, **105**, 213.

46. F. Ma, R. Qu, C. Sun, C. Wang, C. Ji, Y. Zhang and P. Yin, *J. Hazard. Mater.*, 2009, **172**, 792.

47. R. Qu, Y. Niu, J. Liu, C. Sun, Y. Zhang, H. Chen, C. Ji, *React. Funct. Polym.*, 2008, **68**, 1272.

48. Y. C. Chang, S. W. Chang and D. H. Chen, *React. Funct. Polym.*, 2006, **66**, 335.

49. M. Jain, V. K. Garg and K. Kadirvelu, *Bioresource Technol.*, 2011, **102**, 600.

50. M. Tuzen, A. Sari, D. Mendil and M. Soylak, *J. Hazard. Mater.*, 2009, **169**, 263.

51. Y. Z. Niu, R. J. Qu, C. M. Sun, C. H. Wang, H. Chen, C. N. Ji, Y. Zhang, X. Shao and F. L. Bu, *J. Hazard. Mater.*, 2013, **244-45**, 276.

52. J. P. Chen, S. N. Wu and K. H. Chong, *Carbon*, 2003, **41**, 1979.

53. R. J. Qu, C. M. Sun, F. Ma, Y. Zhang, C. N. Ji, Q. Xu, C. H. Wang and H. Chen, *J. Hazard. Mater.*, 2009, **167**, 717.

54. Y. Niu, R. Qu, H. Chen, L. Mu, X. Liu, T. Wang, Y. Zhang and C. Sun, *J. Hazard. Mater.*, 2014, **278**, 267.

55. J. Zhu, X. Zhu, Z. Cheng, F. Liu and J. Lu, *Polymer*, 2002, **43**, 7037.

Table 1

Maximum adsorption capacity (q_e(cal)) and parameters (k, R^2) of pseudo-first-order and pseudo-second-order at various initial MO concentrations

C ($mol \cdot L^{-1}$)	Pseudo-first-order kinetics			Pseudo-second-order kinetics		
	k_1	q_e(cal) ($mg \cdot g^{-1}$)	R^2	k_2	q_e(cal) ($mg \cdot g^{-1}$)	R^2
4×10^{-4}	0.00292	47.75	0.9309	1.019×10^{-4}	75.41	0.9986
8×10^{-4}	0.00202	77.36	0.9651	3.899×10^{-5}	113.12	0.9949
16×10^{-4}	0.00433	98.48	0.9482	6.973×10^{-5}	109.65	0.9963

Table 2

Langmuir parameters and Freundlich parameters at different temperatures

T (^{o}C)	Langmuir parameters			Freundlich parameters		
	q_0 (mg·g^{-1})	K_L L.mg^{-1}	R_L^2	K_F	n	R_F^2
20	108.46	0.0209	0.9997	8.988	2.380	0.9139
30	105.26	0.0151	0.9981	6.308	2.141	0.8956
40	93.55	0.0147	0.9946	5.153	2.074	0.8947

Table 3

D-R isotherm linear equations and parameters for the adsorption of MO onto APAN at different temperatures.

T (K)	Liner equation	k ($mol^2.J^{-2}$)	E ($KJ.mol^{-1}$)	R^2
293.15	$y = -4.229x10^{-9}x + 0.02923$	$4.229x10^{-9}$	10.87	0.9557
303.15	$y = -4.565x10^{-9}x + 0.14136$	$4.565x10^{-9}$	10.47	0.9304
313.15	$y = -4.240x10^{-9}x - 0.01532$	$4.240x10^{-9}$	10.86	0.9263

Table 4

Thermodynamic parameters for the adsorption of MO onto APAN at different temperatures.

T (K)	△G (kJ.mol^{-1})	△H(KJ.mol^{-1})	△S(J.mol^{-1}.K^{-1})
293.15	-16.33		
303.15	-16.41	-13.92	8.23
313.15	-16.50		

Schemes and figures

Scheme 1. The ideal synthesis of APAN-nFs.

Scheme 2. The proposed interaction mechanism between the APAN-nFs and dyes in various pH solution.

Fig. 1. FTIR spectra of the raw PAN-nFs and modified PAN-nFs at various reaction temperatures: (a) raw PAN-nFs and raw PAN-nFs after reaction at (b) 90 ^{o}C, and (c) 110 ^{o}C.

Fig. 2. SEM images of (A), (B) the raw PAN-nFs and (C), (D) APAN-nFs.

Fig. 3. Thermogravimetreic curves for (a) raw PAN-nFs, and modified PAN-nFs at various reaction temperatures (b) 90 ^{o}C, and (c) 110 ^{o}C.

Fig. 4. Adsorption towards different dyes onto APAN-nFs under the same concentration of 4×10^{-4} mmol.mL^{-1} at 20 ^{o}C in aqueous solution.

Fig. 5. Effect of ionic strength and various pH solution on the adsorption capacity of MO onto APAN-nFs.

Fig. 6. Adsorption kinetics of APAN-nFs for methyl orange at various concentrations under 20 ^{o}C.

Fig. 7. (a) Pseudo-first-order kinetic plots for adsorption of methyl orange, (b) Pseudo-second-order kinetic plots for adsorption of methyl orange.

Fig. 8. Isotherm of APAN-nFs for methyl orange at different temperatures.

Fig. 9. (a) Langmuir isotherm of APAN-nFs for methyl orange at different temperatures, (b) Freundlich isotherm of APAN-nFs for methyl orange at different temperatures.

Fig. 10. R_L of APAN-nFs for the adsorption of methyl orange.

Fig. 11. Intraparticle diffusion plot of APAN-nFs for MO.

Fig. 12. The variation of logKc with 1/T.

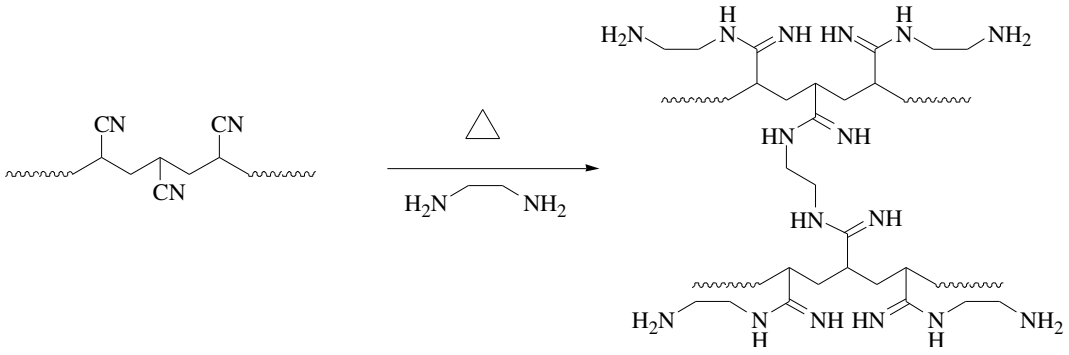

Scheme 1

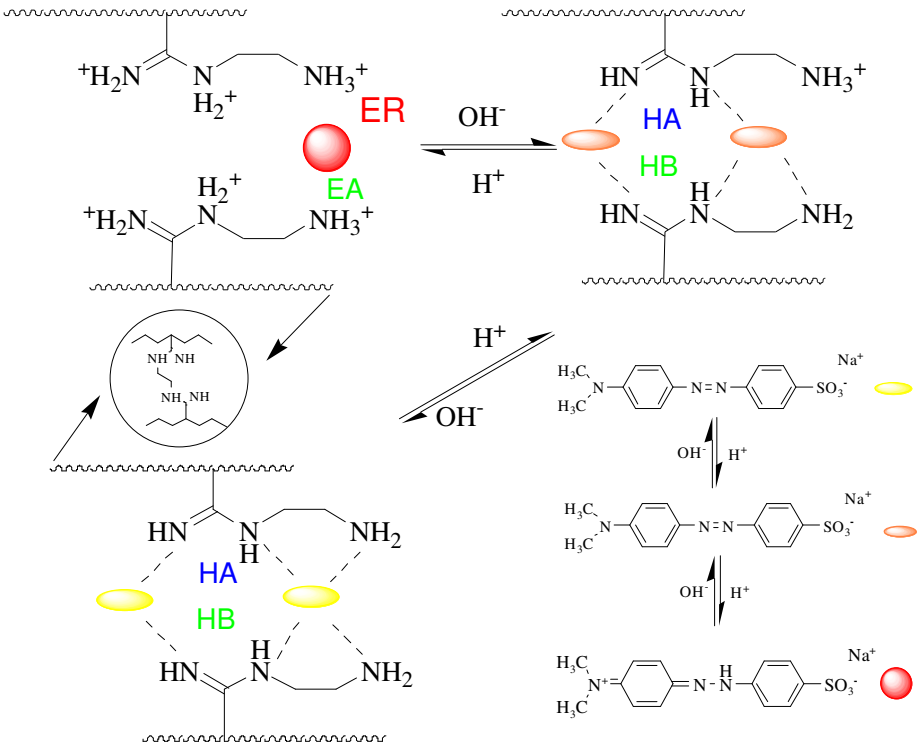

Scheme 2

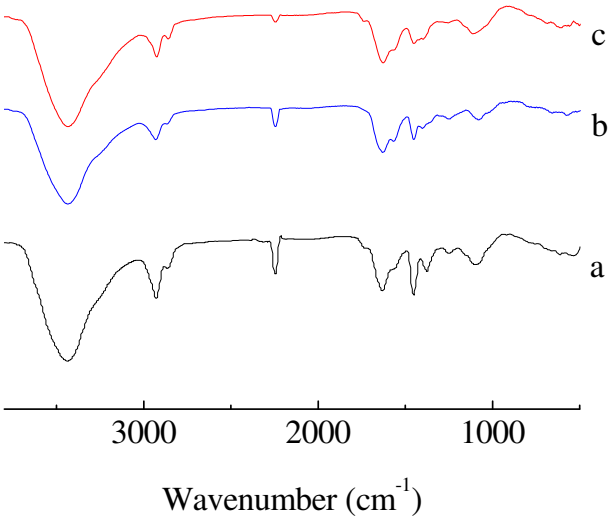

Fig. 1.

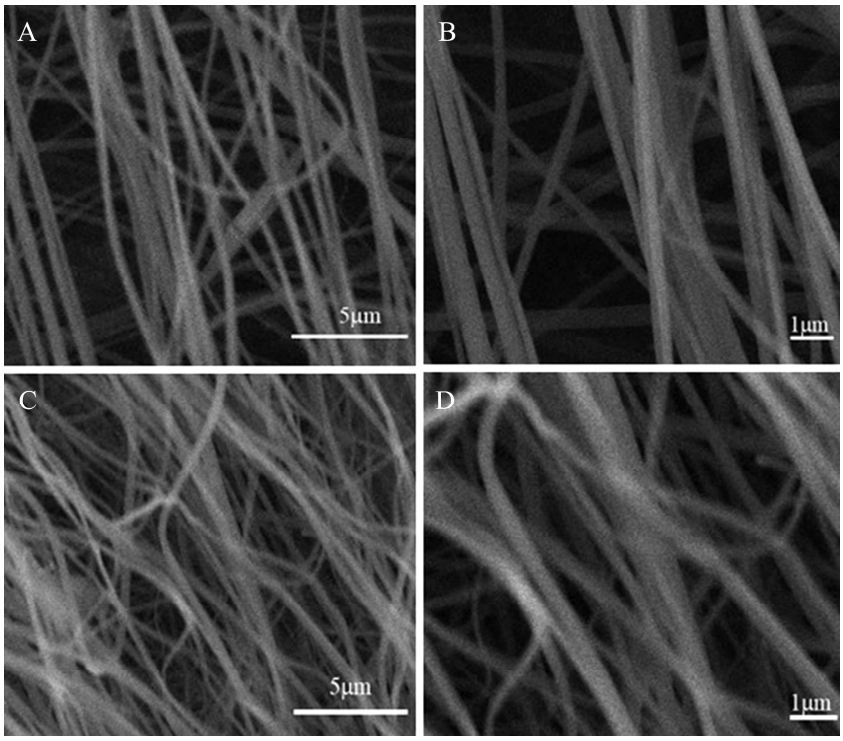

Fig. 2.

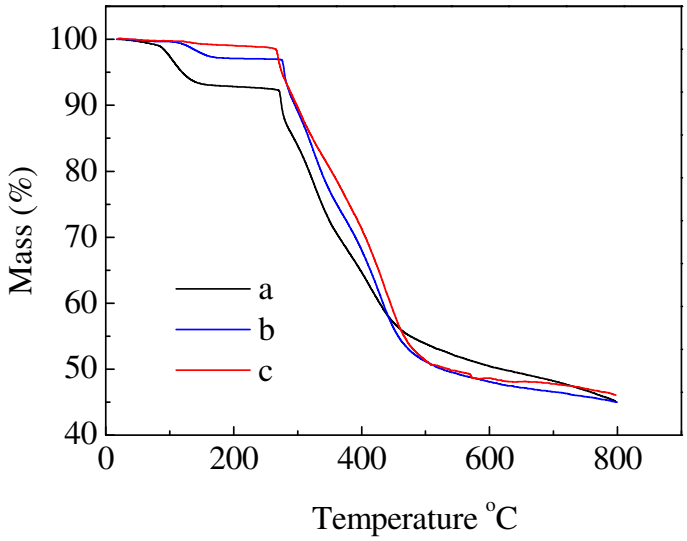

Fig. 3.

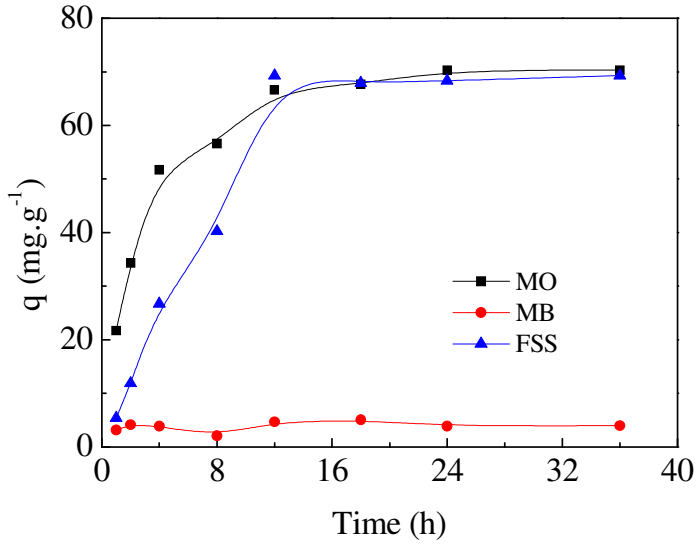

Fig. 4.

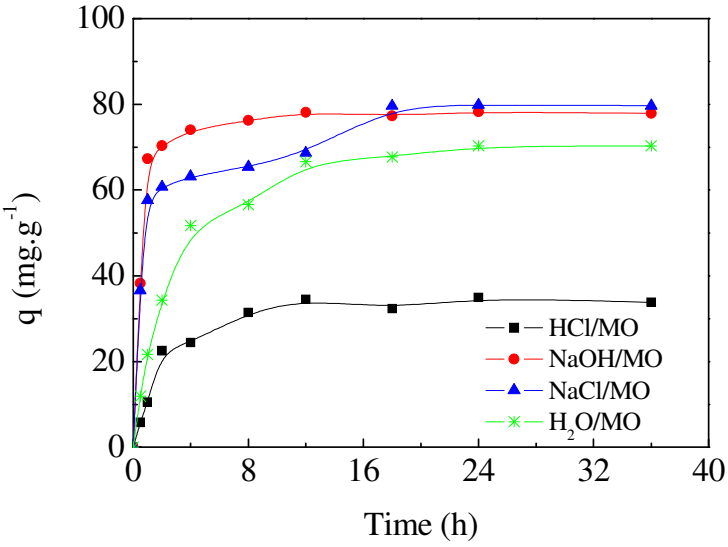

Fig. 5.

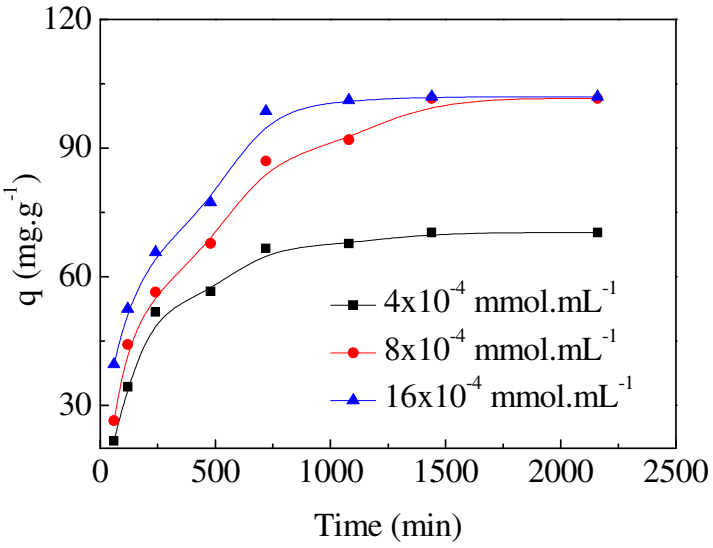

Fig. 6.

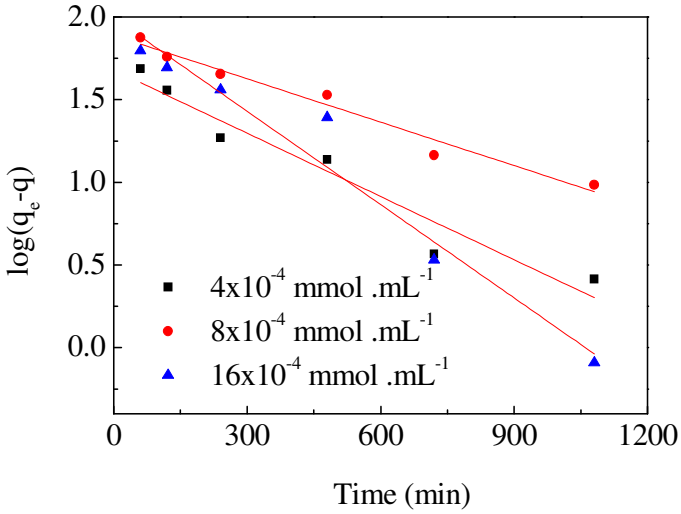

(a)

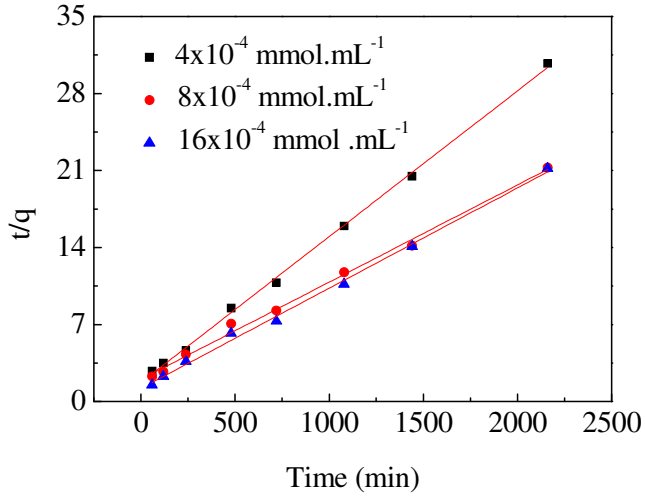

(b)

Fig. 7.

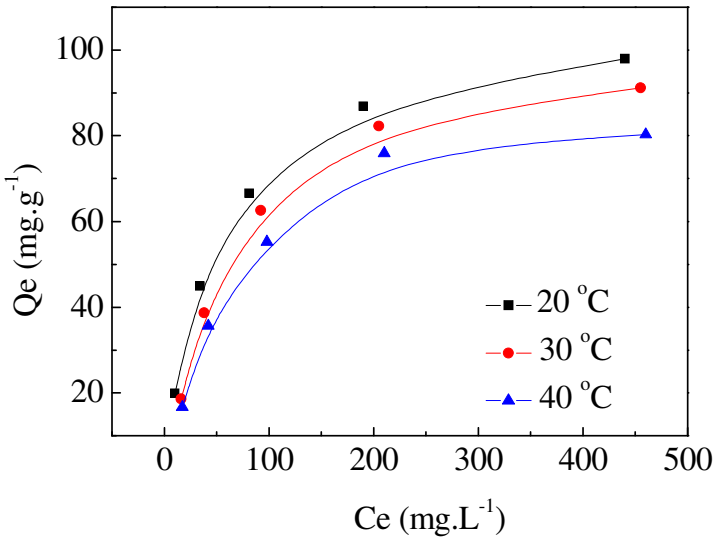

Fig. 8.

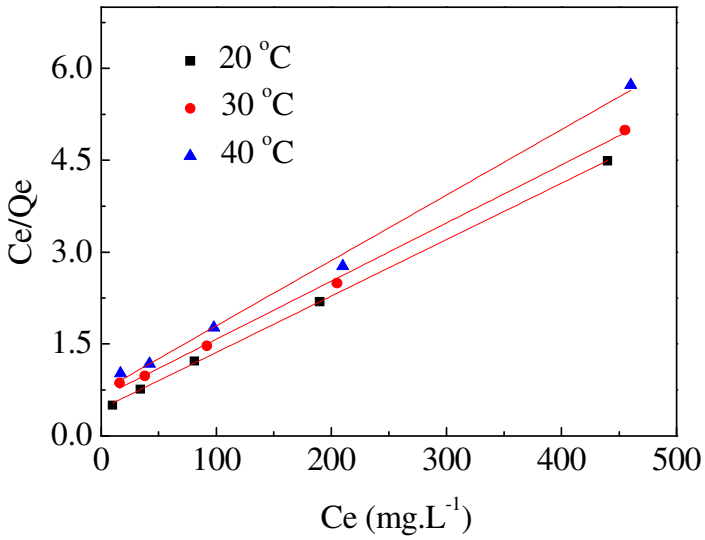

(a)

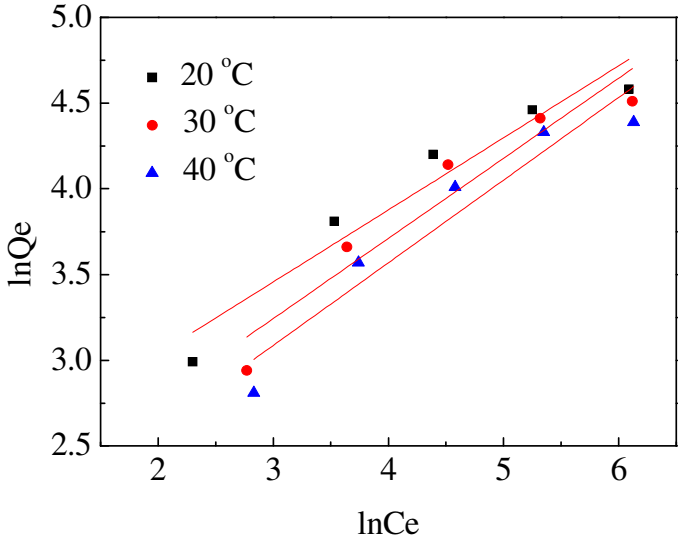

(b)

Fig. 9.

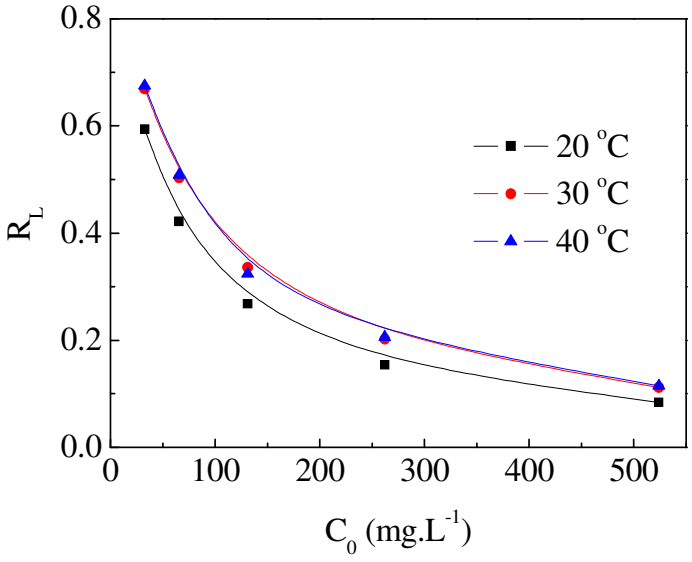

Fig. 10.

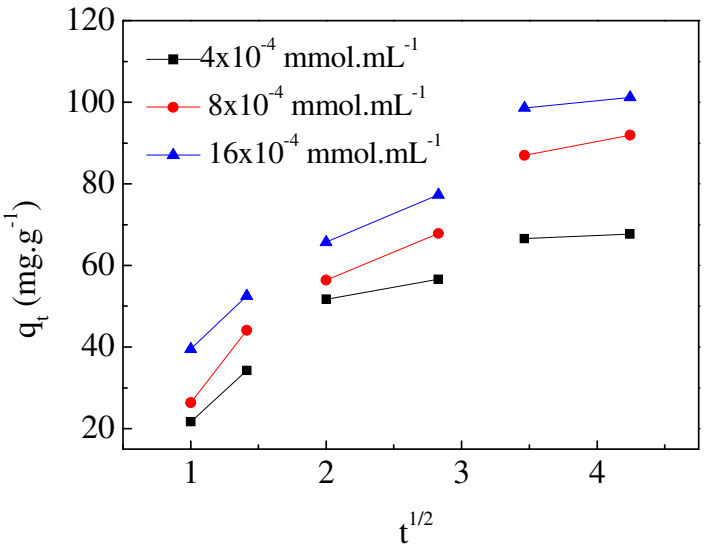

Fig. 11.

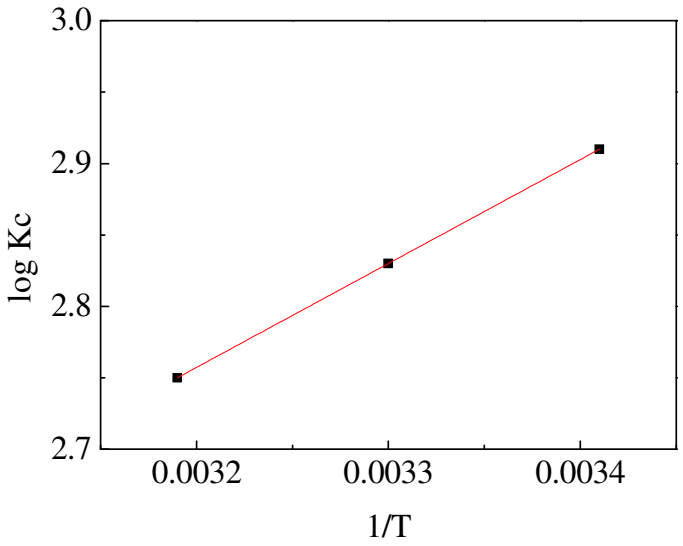

Fig. 12.

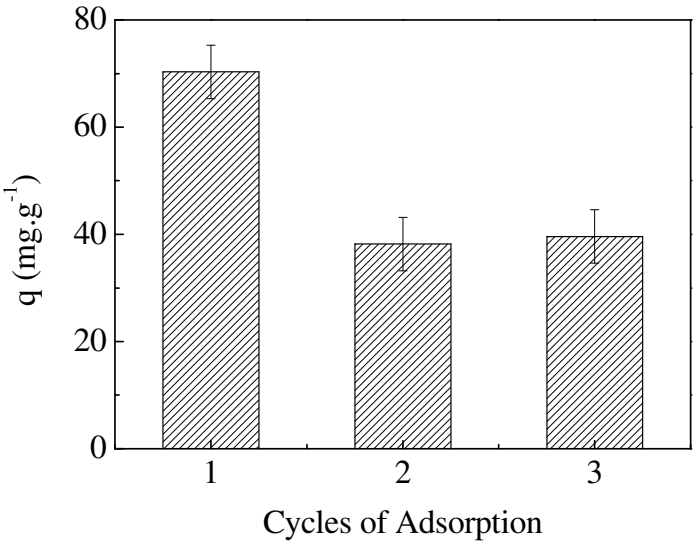

Fig. 13.